

Cooperative and Competitive Spreading Dynamics on the Human Connectome

Highlights

- We use a simple model to study global spreading dynamics on human brain networks
- Hub regions and a backbone of core pathways facilitate early spreading of cascades
- Shortest path structure of brain networks accelerates spreading
- Cascades integrate by converging on polysensory associative areas

Authors

Bratislav Mišić, Richard F. Betzel, Azadeh Nematzadeh, ..., Alessandro Flammini, Yong-Yeol Ahn, Olaf Sporns

Correspondence

osporns@indiana.edu

In Brief

Mišić et al. study how the architecture of human brain networks shapes the spreading of information. They find evidence of several organizational principles that increase the speed of spreading and determine how information cascades become integrated in the brain.



Cooperative and Competitive Spreading Dynamics on the Human Connectome

Bratislav Mišić,^{1,6} Richard F. Betzel,^{1,6} Azadeh Nematzadeh,² Joaquin Goñi,³ Alessandra Griffa,^{4,5} Patric Hagmann,^{4,5} Alessandro Flammini,² Yong-Yeol Ahn,² and Olaf Sporns^{1,3,*}

¹Department of Psychological and Brain Sciences, Indiana University, 1101 E. 10th Street, Bloomington, IN 47405-7007, USA

²School of Informatics and Computing, Indiana University, 919 E. 10th Street, Bloomington, IN 47408, USA

³Indiana University Network Science Institute, Indiana University, 1022 E. 3rd Street, Bloomington, IN 47405, USA

⁴Signal Processing Laboratory (LTS5), Ecole Polytechnique Fédérale de Lausanne, Route Cantonale, 1015 Lausanne, Switzerland

⁵Department of Radiology, Lausanne University Hospital and University of Lausanne, Rue du Bugnon 21, 1011 Lausanne, Switzerland

⁶Co-first author

*Correspondence: osporns@indiana.edu

<http://dx.doi.org/10.1016/j.neuron.2015.05.035>

SUMMARY

Increasingly detailed data on the network topology of neural circuits create a need for theoretical principles that explain how these networks shape neural communication. Here we use a model of cascade spreading to reveal architectural features of human brain networks that facilitate spreading. Using an anatomical brain network derived from high-resolution diffusion spectrum imaging (DSI), we investigate scenarios where perturbations initiated at seed nodes result in global cascades that interact either cooperatively or competitively. We find that hub regions and a backbone of pathways facilitate early spreading, while the shortest path structure of the connectome enables cooperative effects, accelerating the spread of cascades. Finally, competing cascades become integrated by converging on polysensory associative areas. These findings show that the organizational principles of brain networks shape global communication and facilitate integrative function.

INTRODUCTION

Spreading dynamics take place on virtually all real-world networks and systems, from infectious diseases on human contact networks (Pastor-Satorras and Vespignani, 2001) to tweets, memes, and behaviors on social networks (Granovetter, 1978; Centola, 2010). A fundamental question in modern network science is how such spreading dynamics are shaped by the structure of the networks on which they occur (Watts, 2002). Of particular interest is viral spreading, where digital content such as images, videos, or links sweeps through a population by being frequently shared between individuals, leading to widespread adoption. The likelihood, size, and speed of such cascades depend on their point of origin and on the global topology of the network (Nematzadeh et al., 2014).

Recent advances in imaging and tracing of neuronal connections have resulted in the creation of comprehensive network

maps (connectomes) of neural elements and their interconnections, both in animal models (Oh et al., 2014) and in the human brain (Hagmann et al., 2008), revealing a hierarchical community structure (Bassett et al., 2010) and a backbone of densely interconnected hubs (van den Heuvel et al., 2012). The topological properties of the human connectome suggest that one of its primary functions is to support efficient communication and integration of information (Bullmore and Sporns, 2012). As in socio-technological systems, models of brain communication have begun to create links between topology and function (Stam et al., 2015; Mišić et al., 2014b). So far, diffusion models have proven useful for delineating functional modules (Betzel et al., 2013; Delvenne et al., 2010) and predicting statistical dependencies (functional connectivity) among remote neuronal time courses (Goñi et al., 2014).

Here we show that spreading models reveal novel features of brain structure and function. Using an anatomical brain network derived from high-resolution diffusion spectrum imaging (DSI), we investigate the anatomical design principles that shape and constrain spreading on brain networks. We consider three scenarios: a single-seed scenario where a perturbation is initiated at a single location, leading to a single cascade, as well as two different two-seed scenarios, where perturbations are initiated at two locations, leading to either cooperative or competitive cascades. We compare our findings to patterns of functional connectivity derived from fMRI, with a focus on resting state networks (RSNs)—the putative building blocks of higher cognitive functions (Damoiseaux et al., 2006; Smith et al., 2009; Yeo et al., 2011; Power et al., 2011; Fornito et al., 2012).

RESULTS

We simulated network spreading dynamics using a family of linear threshold models (LTMs) that describe how local perturbations trigger global cascades (Granovetter, 1978; O’Dea et al., 2013). The models simulate how multiple exposures to some perturbation from the neighborhood of a node cause the node itself to adopt an active state (Watts, 2002). The threshold parameter is the proportion of a node’s neighbors that must become active before the node itself becomes active. At a threshold of zero, cascades develop along shortest paths, while increasing

the threshold allows cascades to deviate from shortest paths. When the threshold is greater than the inverse of the highest degree in the network, cascades are no longer guaranteed to spread to the whole network. We set the threshold to the highest value at which all perturbations cause a complete cascade, allowing us to focus on adoption times for all possible combinations of nodes. At this threshold, shortest paths only partially predict adoption time ($R^2 = 0.63$) (Figure S2H), i.e., not all cascades spread via topologically shortest paths, with many of them taking advantage of alternative paths as well.

This spreading model maps the initial trajectory of a cascade and does not capture any sustained interaction among neural elements. In other words, the model traces only the immediate effect of one or more instantaneous, coincident perturbations, but does not capture any subsequent feedback or reconfiguration of functional interactions. Although this simple spreading model is not biophysical, the spreading process itself may be thought of in terms of synchronization (Fries et al., 2001; Zhou et al., 2006; Womelsdorf et al., 2007). If many neighbors of a node enter into a particular oscillatory regime, they act as an external synchronizing force on that node. The resulting transient, coherent mode could act much like a balanced branching process (Beggs and Plenz, 2003), thus leading to an oscillatory cascade (Roberts et al., 2015).

Single Seed

We first consider the case where a perturbation is initiated at a single seed node (Figure 1A). Across all possible starting points, cascades spread faster to nodes that are within the same hemisphere (4.97 versus 5.72, $p < 0.001$) and within the same anatomically defined community as the seed node (3.86 versus 5.52, $p < 0.001$) (Figure 1B), with much of the variance in adoption times accounted for by path length. The mean adoption time for a source node (influence) and for a target node (receptiveness) are positively correlated ($r = 0.83$, $p < 0.001$), as high-degree nodes are both efficient at seeding cascades and among the first to be reached by spreading cascades (see Figure S4 for a complete set of correlations between all measures).

Given that much of the present spreading is dominated by shortest paths, we investigated the degree to which the present spreading model is related to network communicability, which takes into account all possible routes between two nodes, with longer routes weighted less (Estrada and Hatano, 2008). Comparing communicability of all node pairs with the adoption times between them, we find a negative relationship ($r^2 = -0.77$; Figure S2), reflecting the fact that node pairs that are more communicable will also have shorter adoption times.

To investigate spreading within and between functional communities (RSNs; Figure S1B), we derive the mean adoption times for sources and targets placed in different RSNs and express them as Z scores relative to a null distribution constructed by randomly permuting RSN assignments within each hemisphere (Figure 1C). Most of the entries in this adoption time matrix are significantly different from chance ($p < 0.05$, Bonferroni corrected), suggesting that the organization and functional relationships among the RSNs reflect a specific, highly organized set of spreading patterns. We find that cascades spread significantly slower between sensory RSNs (somato-motor, visual, and

ventral attention networks) and faster between multimodal RSNs (fronto-parietal, default mode networks).

To investigate the role of individual edges (representing white-matter pathways), we define transit times as the ratio of edge length to edge density, such that short, strong edges have relatively shorter transit times, and long, thin edges have relatively longer transit times. We then use asynchronous updating to resolve the time at which connections are used to spread the cascade (see Experimental Procedures). Early spreading, on average, is driven by a compact backbone of pathways that interconnect a set of medial cortical regions (e.g., medial orbitofrontal and posterior cingulate cortex), as well as the bilateral insulae, while later spreading is completed along more lateral pathways (Figure 1D). It is noteworthy that these regions strongly overlap with the putative rich club of hubs, a central component of the connectome that is hypothesized to support functional integration (van den Heuvel et al., 2012). The edge-betweenness is a good, but imperfect, predictor of the overall use of that edge (Figure 1E). This is consistent with the notion that shortest paths account for the trajectory of many cascades, but that spreading may occasionally proceed via longer paths as well.

Given that connectome density may vary depending on the resolution of the parcellation, the diffusion protocol, and the tractography algorithm, we sought to verify that relative spreading metrics are robust to differences in network density. Following the method described in Experimental Procedures, we generated two additional networks, with densities equal to 1 SD below the population mean ($k = 21,980$ edges, 2.20% density), and 1 SD above ($k = 26,616$ edges, 2.66% density), in addition to the original structural network, the density of which was matched to the population mean ($k = 24,302$ edges, 2.43% density). Adoption times were highly correlated for the three matrices ($r = 0.96$, 0.93, and 0.96), suggesting that relative differences in spreading dynamics are not sensitive to changes in density.

Cooperative Interactions

We next consider the scenario where two perturbations initiated at different seed nodes interact cooperatively (Figure 2A). In principle, triggering a cascade from two nodes simultaneously may lead to accelerated spreading and a speed-up of adoption times across the network. Focusing on these synergistic effects of simultaneous perturbations, we calculate the percent speed-up in adoption time in the two-seed case relative to the faster of the two individual single-seed cases.

Figure 2B shows the mean speed-up across the whole network for all possible seed combinations. The results demonstrate that the greatest global speed-ups are typically observed when the seeds belong to different hemispheres (7.3% versus 9.8%, $p < 0.001$) and communities (5.1% versus 9.0%, $p < 0.001$), while initiating perturbations within the same hemisphere or anatomical community yield little or no speed-up. Figure 2C reveals that the magnitude of a speed-up achieved by any given pair of seeds can be predicted by their topological relationship. First, speed-ups are significantly greater for pairs of nodes that are not linked by an anatomical connection compared to those that are ($p < 0.001$). Second, speed-ups vary in proportion to the path length between seeds, such that the greatest cooperative effects can be achieved if the cascades are initiated far

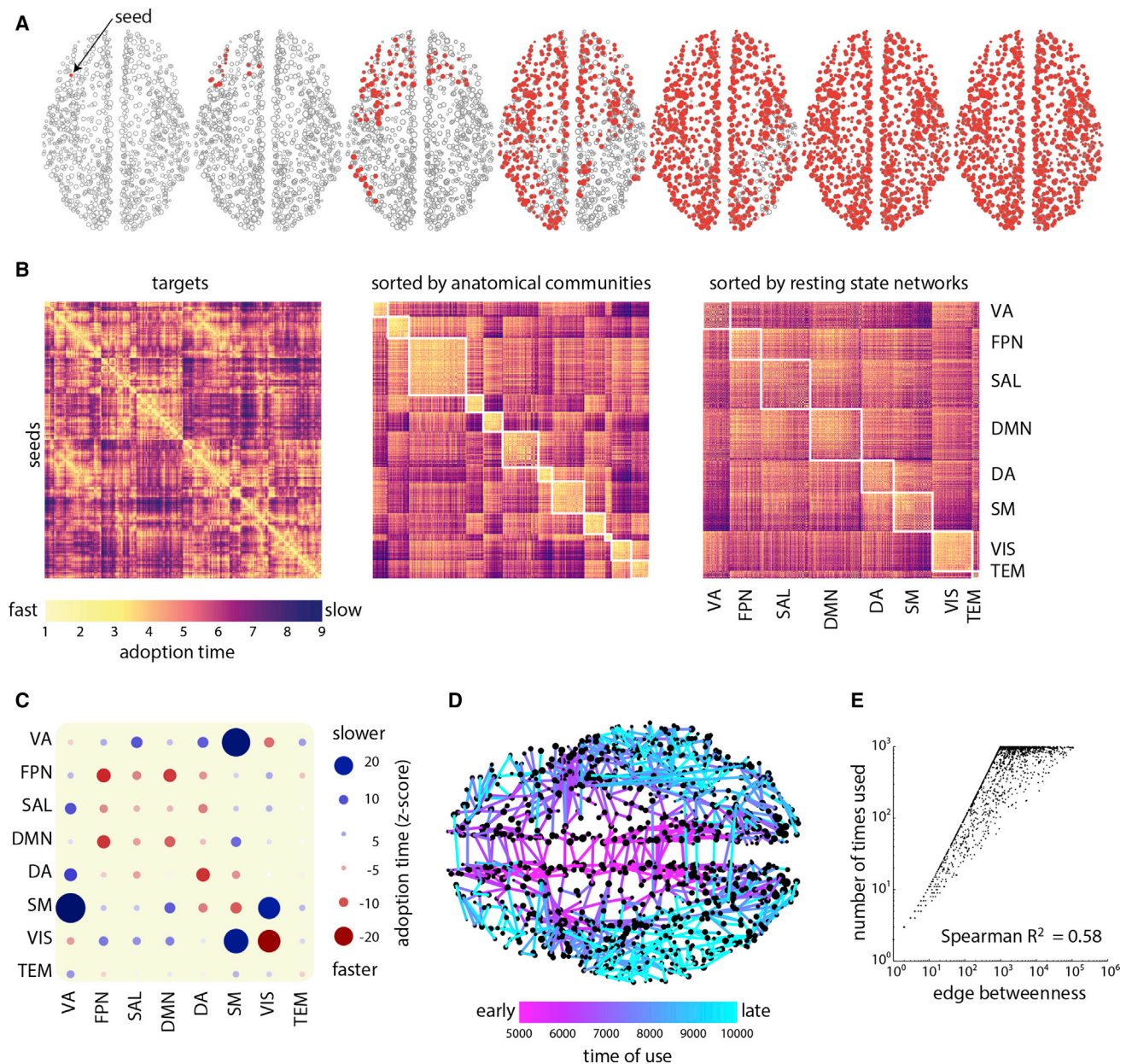


Figure 1. Single-Seed Spreading

(A) Schematic showing how a single perturbation (indicated by the arrow) develops into a global cascade.

(B) Adoption time matrices, showing the time it takes for a perturbation initiated at a particular seed node (rows) to reach another node in the network (columns). Matrices are arranged by hemisphere (left), anatomical communities (middle), and resting state networks (right: ventral attention, VA; fronto-parietal, FPN; salience, SAL; default mode, DMN; dorsal attention, DA; somato-motor, SM; visual, VIS; temporal, TEM).

(C) Mean adoption times between resting state networks, expressed as Z scores relative to a null distribution in which the assignment of nodes is permuted (within-hemisphere). Blue circles indicate that the adoption times are slower than the null distribution, while red circles indicate the adoption times are faster.

(D) Connections that are used across all possible seeds and the average times at which they are used. Warmer colors indicate earlier contributions to the cascade.

(E) Relationship between edge-betweenness and the number of times an edge is used.

from one another. Third, for seeds that share a connection, the greatest speed-ups are achieved if both seeds are high-degree members of the putative rich club of hubs (van den Heuvel et al., 2012). These cooperative effects engender several synergistic relationships among the RSNs, most notably between the

somato-motor and ventral attention networks, the somato-motor and visual networks, and the visual and fronto-parietal networks (Figure 2D).

The cooperative scenario also allows us to ask which parts of the brain benefit from the greatest local speed-ups. Averaging

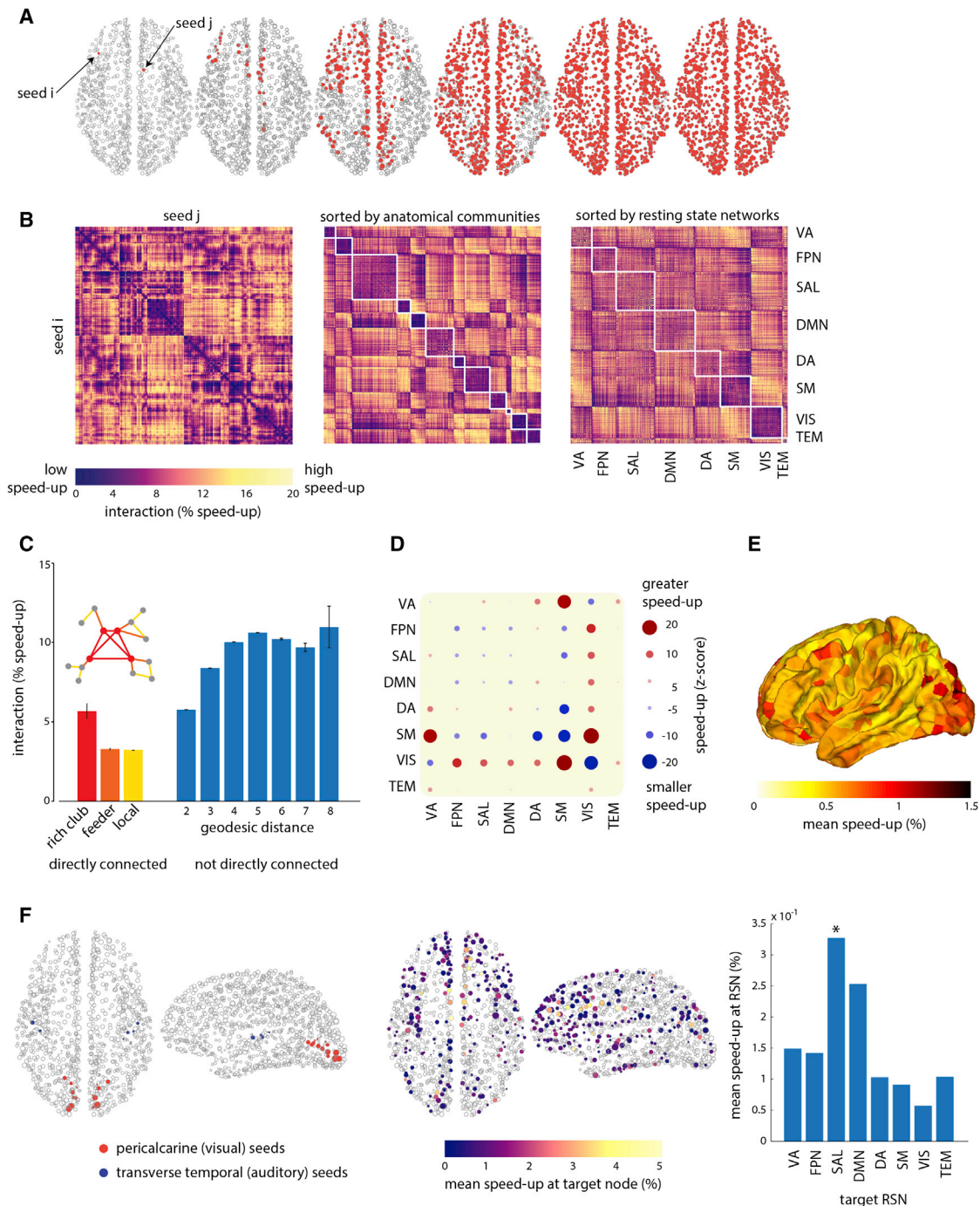


Figure 2. Cooperative Spreading

(A) Schematic showing how two simultaneous perturbations (indicated by arrows) combine into a global cascade.

(B) Speed-up matrices, showing how much faster the two-seed scenario is compared to the faster of the comparable one-seed scenarios. Matrices are arranged by hemisphere (left), anatomical communities (middle), and resting state networks (right).

(C) Relationship between two seeds (structural connectivity, geodesic distance) predicts the magnitude of the speed-up. Error bars represent SE.

(D) Mean speed-ups between resting state networks, expressed as Z scores relative to a null distribution in which the assignment of nodes is permuted (within-hemisphere). Blue circles indicate that the speed-ups are smaller than expected by chance, while red circles indicate the speed-ups are faster.

(E) The mean speed-up experienced by individual brain regions, averaged across all seed combinations.

(F) A specific test case, where all possible combinations of primary visual (pericalcarine) and primary auditory (transverse temporal) nodes are seeded. The resulting speed-ups are observed primarily in the salience network. The bar graph indicates the speed-ups for all RSNs (statistically significant speed-ups, as determined by permutation tests, are indicated by an asterisk).

across all possible seed combinations, we find that polysensory associative areas exhibit the greatest synergistic effects (Figure 2E), including the posterior portion of the temporoparietal junction and the intraparietal sulcus, which suggests that the well-known integrative and coordinative functions of these areas may arise from their network embedding, which promotes cooperative spreading dynamics. Figure 2F shows a set of specific test cases, where we seed perturbations in primary visual (pericalcarine) and primary auditory (transverse temporal) cortices. The resulting speed-ups are distributed across the brain, with peak effects including the insulae and anterior cingulate. Across RSNs, we find that the salience network experiences a statistically significant speed-up ($p < 0.01$, Bonferroni corrected), consistent with its role as an attentional subsystem that responds to behaviorally salient events (Seeley et al., 2007; Menon and Uddin, 2010).

Competitive Interactions

Finally, we consider the scenario in which two perturbations result in two cascades, representing competing or complementary neural signals (Figure 3A). These dynamics are described as “competitive” because the two cascades effectively compete for influence over the nodes of the network: a node may adopt one of two states, but not both. Thus, competitive dynamics presented here should not be confused with neuronal inhibition or lateral inhibition. Although the competitive mechanism described in the present study bears some similarity to the notion of biased competition in selective attention (Koch and Ullman, 1987; Desimone and Duncan, 1995), it is considerably more general, in the sense that cascades may originate from any type of local perturbation (not just those related to sensory transduction), and it does not include any overt, top-down inhibitory mechanism.

We first characterize the competition between cascades by introducing two metrics: diversity and competitiveness. As competing cascades envelop the brain, they eventually meet and form one or more fronts. To delineate these fronts and determine where competing cascades tend to interface with each other, we estimate the diversity of a node as the entropy of its neighborhood (see Experimental Procedures). Nodes whose neighbors have all adopted the same state and are part of the same cascade will have low diversity, while nodes whose neighbors are equally distributed among the two cascades will have high diversity. We find that nodes comprising multimodal association RSNs—particularly the default mode, dorsal attention, and fronto-parietal networks—tend to have the most diverse neighborhoods (Figures 3B and 3C). These diverse neighborhoods define the fronts where competing cascades converge, providing opportunities for their effective integration.

We define the competitiveness of a node as the average cascade size for perturbations initiated at that node, averaged across all other competing nodes. Thus, highly competitive nodes are those that initiate the largest cascades regardless of where the other perturbation is seeded. The model predicts that the diverse multimodal RSNs will be the most competitive, suggesting that association networks tend to dominate spreading dynamics (Figures 3D and 3E). At the level of individual nodes, we find several consistent “hot spots,” including the su-

perior frontal gyrus, insula, superior temporal gyrus, and posterior parietal cortex, that tend to be both competitive and diverse, consistent with empirical findings indicating that these higher-order brain areas are topologically central and receive polysensory input from multiple sources (Hagmann et al., 2008; Menon and Uddin, 2010). Diversity and competitiveness are positively correlated ($r = 0.65$, $p < 0.01$), as high-degree hubs have both diverse neighborhoods and out-compete nodes with lower degrees (see Figure S4 for a complete set of correlations between all measures).

To estimate the degree to which a node conforms to its neighborhood, we calculate the probability of the node’s allegiance (i.e., its final state) given the final allegiance of its neighbors. Node conformity was uniformly greater than 0.5, suggesting that nodes tend to adopt the same state as their neighbors. Importantly, node conformity was anticorrelated with degree ($r^2 = 0.43$, $p < 0.001$; Figures 3F and 3G), indicating that while poorly connected nodes are more likely to adopt the same state as their neighbors, high-degree hubs often differ from their neighbors. This propensity for dissent is due to the fact that hubs tend to be early adopters (Figure S2A); thus, their allegiance tends to be more independent of their neighbors compared to low-degree nodes. By comparison, low-degree nodes tend to adopt late in the cascade and are more likely to be influenced by their neighborhood.

Finally, the competitive scenario allows us to determine whether spreading dynamics are capable of predicting functional connectivity. Specifically, we can operationalize functional connectivity between two nodes in terms of how often, on average, they participate in the same cascade. If two nodes participate in the same cascade across many different seeding scenarios, this suggests an overlap in their functional profile and should be predictive of their functional connectivity. We therefore extended the competitive spreading model beyond the two-seed scenario, to consider multiple seeds that compete with each other. In the two-seed case it is possible to exhaustively test every single combination, but the number of possible combinations increases exponentially with the number of seeds, making it intractable to exhaustively sample all combinations. Thus, for each n -seed scenario we ran 10,000 seed combinations, which we randomly sampled, without replacement, from the larger space of all possible combinations. For each such n -seed scenario, we calculated an “association weight” for each pair of nodes: the number of times (out of 10,000) that the node pair participates in the same cascade. This association weight is effectively a proxy for functional connectivity, as it represents the overlap in functional profiles for a pair of nodes. Finally, for each n -seed scenario we calculated the correlation between the association weight and the observed functional connectivity matrices.

We performed this procedure for a range of scenarios, from $n = 2$ to $n = 80$ seeds. As the number of seeds increases, so does the correlation between association weight and functional connectivity (Figure 4A). Importantly, there is a clear peak in the correlation when the number of seeds equals 25 ($r = 0.41$). Figure 4B shows a visual comparison between the empirical functional connectivity matrix and the association weight matrix, while Figure 4C shows the edge-wise relationship

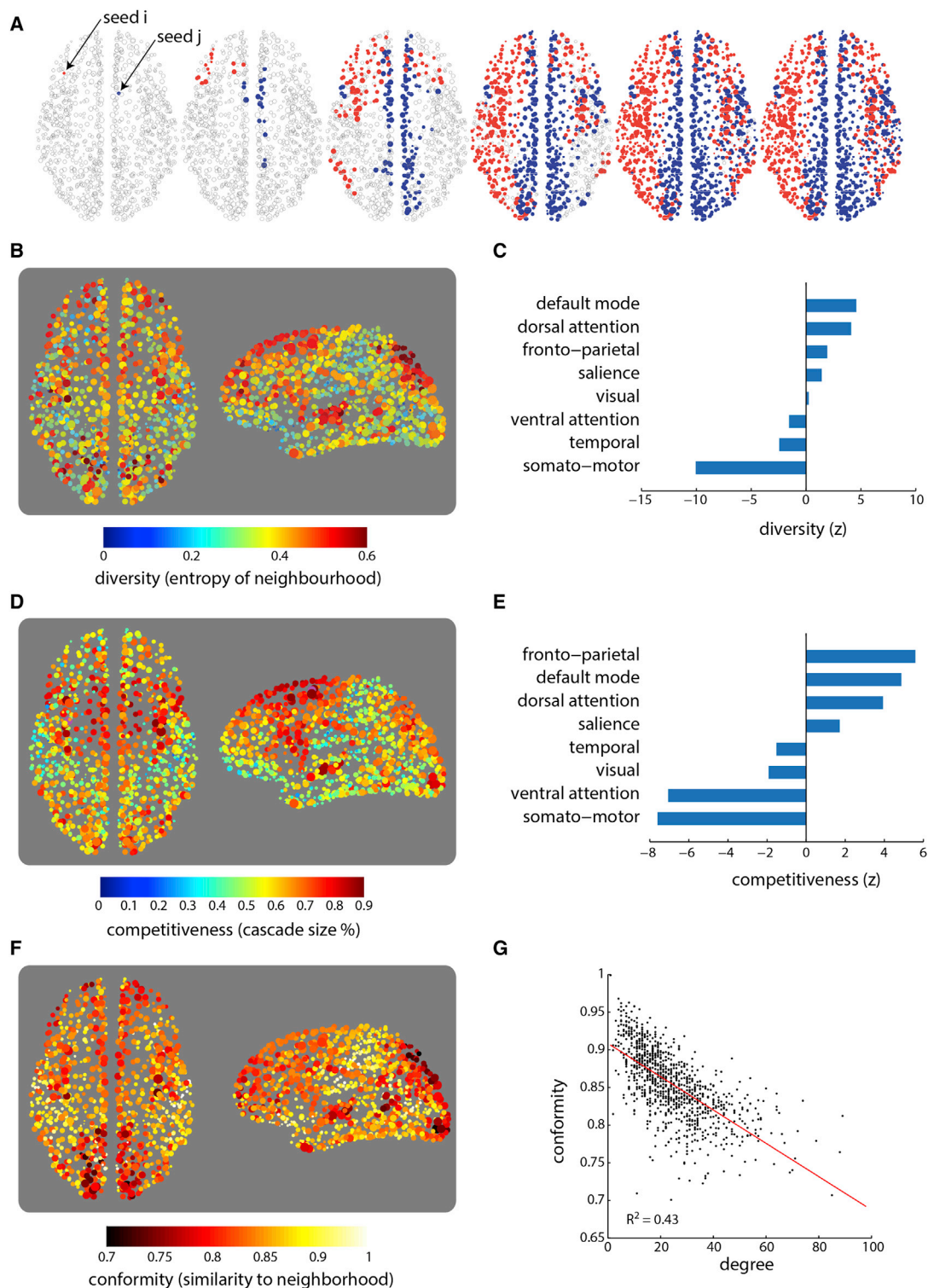


Figure 3. Competitive Spreading

(A) Schematic showing how two simultaneous perturbations (indicated by arrows) develop into competing cascades.

(B, D, and F) The competitiveness, diversity, and conformity of individual nodes.

(C and E) The mean competitiveness and diversity of resting state networks, expressed as a Z score relative to a null distribution in which the assignment of nodes is permuted. Positive Z scores indicate greater competitiveness and diversity than expected by chance.

(G) Relationship between node degree and conformity.

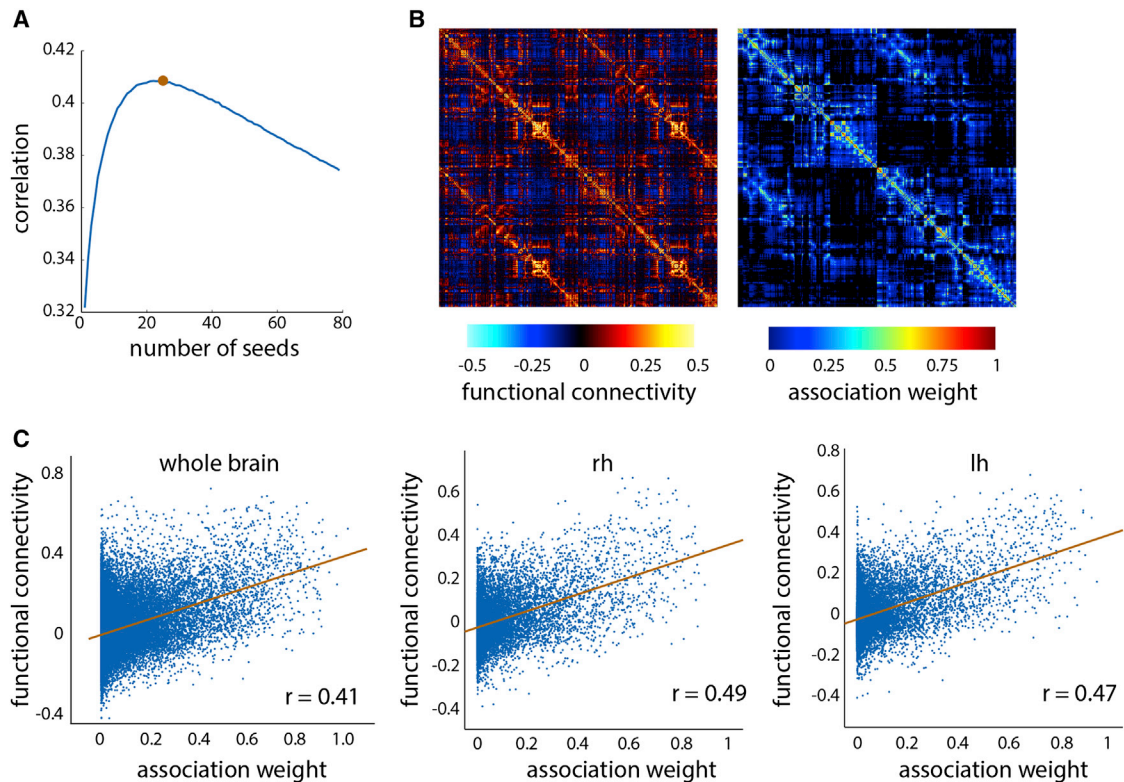


Figure 4. Predicting Functional Connectivity

For the n -seed competitive scenario, functional connectivity is operationalized as the proportion of times two nodes participate in the same cascade (“association weight”).

(A) Relationship between the number of seeds and the correlation between empirical and predicted functional connectivity.

(B) Empirical and predicted functional connectivity matrices.

(C) Edge-wise relationship between empirical and predicted functional connectivity, for the whole brain, as well as for individual hemispheres (rh, right hemisphere; lh, left hemisphere).

between association weight and empirical functional connectivity ($r = 0.41$). Overall, these correlations between predicted and empirical functional connectivity compare favorably to many other computational “forward” models, including neural mass models (Honey et al., 2009), random walk/diffusion models (Betzel et al., 2013; Abdelnour et al., 2014), and routing models (Goñi et al., 2014). Similar to those models, the present spreading model is even better at predicting functional connectivity for single hemispheres ($r = 0.47$ for left, $r = 0.49$ for right), most likely due to the inherent limitations of computational tractography for inferring inter-hemispheric anatomical projections (see [Methodological Considerations](#) for more discussion).

DISCUSSION

In summary, these findings offer a dynamic view of spreading processes on the human connectome. The connectivity of the brain shapes and constrains spreading patterns, revealing a set of anatomical design principles underlying the emergence of global dynamics. In particular, the present report demonstrates that (i) rapid spreading is mainly facilitated by a compact core of high-degree hubs and central paths, (ii) cooperative relationships among RSNs are enabled by the shortest path

structure of the network, and (iii) the associative properties of polysensory areas and subnetworks arise from their ability to integrate multiple cascades. These architectural features give rise to highly organized spreading patterns, including functionally relevant interplay between RSNs. The three scenarios presented here—single seed, cooperative, and competitive spreading—open new perspectives on the coexistence of functional segregation and integration in brain networks.

Network Structure Shapes Spreading

Our results reveal that hubs and a backbone of pathways dominate early spreading, serving to outline the configuration of the resulting cascade. These data contribute to growing literature on the importance of hub nodes, which are disproportionately important in multiple cognitive domains (Cole et al., 2013; Fornito et al., 2012; Crossley et al., 2013), while disruption of hub connectivity is increasingly recognized as a hallmark of neurological and psychiatric disorders (Rubinov and Bullmore, 2013; Stam, 2014). Likewise, the pathways that support early spreading are reminiscent of a high-capacity backbone of pathways reported in previous studies (van den Heuvel et al., 2012). These findings offer a possible explanation for why hubs and central pathways are so important: across all possible starting points, cascades

spread along a specific set of trajectories that revolve around hub nodes, which effectively set the pace for spreading and establish the initial outline of the cascade. This propensity for spreading via central hubs and pathways further predicts that anatomical hubs should be functional hubs as well, consistent with previous reports on structure-function relationships in the brain (Honey et al., 2009; Shen et al., 2015).

In addition, the shortest path structure of the network is shown to be a key architectural feature that shapes spreading patterns and determines the relationships between components of the network. In particular, the shortest path structure of the network helps to accelerate the spread of cascades, enabling cooperative effects. The shortest path structure has always been problematic for theoretical models of brain function because communication along shortest paths entails the biologically implausible assumption that neural elements or signals possess complete knowledge of the global topology. In the present model, cascades naturally spread along shortest paths without any such knowledge, providing a biologically plausible mechanism for how neural communication may take advantage of the shortest paths in the network.

The effect of network structure is particularly salient in the cooperative and competitive relationships between RSNs. Functional interactions between RSNs are an active topic of research (Zalesky et al., 2014), with many cognitive functions supported by dynamic coordination between functional modules, including attention (Hellyer et al., 2014) and memory (Fornito et al., 2012; Kragel and Polyn, 2015). Our results demonstrate that a simple spreading process that takes place on an anatomically realistic network predicts the existence of such relationships between RSNs. For instance, the model predicts a synergistic relationship between the visual and somato-motor networks, consistent with the notion that these two networks must coordinate to effect multisensory perception and motor control. In addition, we find that polysensory associative areas (precuneus, posterior cingulate, insula) and networks (default mode, frontoparietal, salience) tend to have diverse neighborhoods, which is consistent with their putative role in functional integration.

The Role of Simple Models

Our approach highlights the promise and potential utility of communication and spreading models for illuminating principles of brain structure and function. By deliberately abstracting away microscopic details such as neuronal signaling, simple models emphasize the emergence of global patterns from the interactions among individual neural elements and allow us to articulate and quantify the behavior of the system as a whole (Raj et al., 2012; Stam et al., 2015; O’Dea et al., 2013; Misić et al., 2014a, 2014b; Messé et al., 2015). This approach is complementary to traditional modeling paradigms in computational neuroscience, which aim to reduce large populations of spiking neurons to a distribution of states across time (Deco et al., 2008; Ritter et al., 2013). By modeling the interactions between neuronal populations, these traditional paradigms reveal the emergence and perpetual reconfiguration of coherent functional networks (Deco et al., 2011). In comparison, the present “single shot” spreading model maps the initial trajectory of a focal perturbation and provides complementary information

about the role of network connectivity in shaping functional integration.

The simple spreading model described in the present report can be readily extended to address specific experimental questions and to generate testable predictions. We envision the model as a “workbench” for investigating specific types and combinations of perturbations and addressing questions regarding sensation, perception, motor control, and higher cognitive function. For instance, in the present report we demonstrated one such test case, where two perturbations were initiated in primary auditory and primary visual cortex, representing multisensory stimulation. Our model predicted that this auditory-visual stimulation primarily benefits the salience network: an attentional subsystem for orienting attention to external events. Similarly, our model predicted that the majority of cascades propagate via hub nodes and a compact core of medial projections. This result suggests that structural hubs also tend to be functional hubs because they mediate the spread of cascades and could be experimentally verified by comparison with stimulation studies.

More generally, simple spreading models can be used to simulate any perturbation of interest. For example, researchers interested in visual control of movement and sensory-motor integration could simultaneously initiate perturbations in primary visual cortex and primary motor cortex (Wolpert and Ghahramani, 2000). The predictions of the model, such as which areas benefit most from cooperative spreading, could then be tested against recordings of local neural activity, such as electrocortigraphy or intracranial electroencephalography, or source-localized magnetoencephalography. Likewise, researchers can use the model to investigate how RSNs interact to implement tasks and behavior (Fornito et al., 2012). A number of recent studies have posited that flexible switching based on external task demand is mediated by parts of the frontoparietal control network (Cole et al., 2013). Investigators interested in the role of this control network could systematically test how quickly cascades spread with and without the presence of the frontoparietal network. The predictions from these simulations, such as adoption times, could be linked to human behavior by correlating adoption times with individual differences in task-switching performance.

Methodological Considerations

Following in the footsteps of minimal models of other complex systems, such as group dynamics, flocking and swarming (Vicsek et al., 1995; Couzin et al., 2005), traffic patterns and crowd panic (Helbing et al., 2000), epidemics (Pastor-Satorras and Vespignani, 2001), and social collective behavior (Schelling, 1971; Henry et al., 2011), the present model trades off biological detail for the ability to capture the emergence of global patterns. Despite several parallels with mesoscopic neural dynamics, this general spreading model does not explicitly embody any details about neural physiology. Rather, we have used the spreading model as a tool to explore the complex architecture of the human connectome and to generate relative metrics about its ability to support communication.

Another potential limitation of the present study is the use of diffusion imaging and computational tractography for inferring

anatomical connectivity. At present, the combination of DSI and tractography is the leading approach for non-invasive in vivo reconstruction of human anatomical connectivity. However, this approach has several known limitations, including the inability to perfectly resolve crossing fibers and a susceptibility to both false positives and false negatives, resulting in diminished anatomical accuracy (Jones et al., 2013; Thomas et al., 2014), which may be reflected in our results. Although our use of a group-composite matrix may attenuate single-subject-level inaccuracies, this does not address any potential systematic biases in the reconstruction procedure. These shortcomings of diffusion imaging and tractography highlight the need for new non-invasive technologies for mapping anatomical brain networks in humans.

Conclusion

As the field of connectomics advances toward a more complete structural description of the human brain (Insel et al., 2013; Van Essen et al., 2013), these models may contribute to a much-needed theoretical framework for studying how communication processes unfold within the global topology. Akin to their role in other areas of contemporary science, such as group dynamics (Vicsek et al., 1995; Couzin et al., 2005), sociology (Helbing et al., 2000; Schelling, 1971; Henry et al., 2011), and epidemiology (Pastor-Satorras and Vespignani, 2001), spreading models of brain function may allow us to capture the organizational principles of the connectome by bringing into focus the emergent global behavior of the system.

EXPERIMENTAL PROCEDURES

Data Acquisition

Informed written consent in accordance with institutional guidelines (protocol approved by the Ethics Committee of Clinical Research of the Faculty of Biology and Medicine, University of Lausanne, Switzerland) was obtained for all subjects. A total of 40 healthy participants (16 females, 25.3 ± 4.9 years old) were scanned in a 3-Tesla MRI scanner (Trio, Siemens Medical, Germany) using a 32-channel head-coil. The session protocol was comprised of (1) a magnetization-prepared rapid acquisition gradient echo (MPRAGE) sequence sensitive to white/gray matter contrast (1-mm in-plane resolution, 1.2-mm slice thickness), (2) a DSI sequence (128 diffusion-weighted volumes and a single b_0 volume, maximum b -value $8,000 \text{ s/mm}^2$, $2.2 \times 2.2 \times 3.0 \text{ mm}$ voxel size), and (3) a gradient echo EPI sequence sensitive to BOLD contrast (3.3-mm in-plane resolution and slice thickness with a 0.3-mm gap, TR 1,920 ms, resulting in 280 images per participant). During the fMRI scan, participants were not engaged in any overt task, and the scan was treated as eyes-open resting-state fMRI (rs-fMRI).

Data Pre-processing

Initial signal processing of all MPRAGE, DSI, and rs-fMRI data was performed using the Connectome Mapper pipeline (Daducci et al., 2012). Gray and white matter were segmented from the MPRAGE volume. The resulting gray matter volume was divided into 1,015 approximately equally sized regions of interest (Cammoun et al., 2012). The focus of the present study was on cortical structures only, so all subcortical regions were discarded from further analysis, including bilateral amygdala, hippocampus, thalamus, caudate, putamen, nucleus accumbens, pallidum, and the brain stem, resulting in 1,000 regions of interest. Each region of interest could be mapped to 1 of 68 cortical areas (34 in each hemisphere).

DSI data were reconstructed following the protocol described by Wedeen et al. (2005), allowing us to estimate multiple diffusion directions per voxel. The diffusion probability density function was reconstructed as the discrete

3D Fourier transform of the signal modulus. The orientation distribution function (ODF), ϕ , was calculated as the radial summation of the normalized 3D probability distribution function $\rho(x)$

$$\phi(\mathbf{u}) = \int \rho(\rho\mathbf{u})\rho^2 d\rho, \quad (\text{Equation 1})$$

where ρ is the radius and \mathbf{u} a unit vector. Thus, the ODF is defined on a discrete sphere and captures the diffusion intensity in every direction. The integral was evaluated for a set of vectors \mathbf{u}_i representing the vertices of a tessellated sphere, resulting in a diffusion map composed of ODFs at every location in the brain. These functions represent deformed spheres with radius proportional to $\phi(\mathbf{u})$.

Structural Connectivity

Structural connectivity matrices were estimated for individual participants using deterministic streamline tractography on reconstructed DSI data, initiating 32 streamline propagations per diffusion direction, per white matter voxel (Wedeen et al., 2008). Within each voxel, the starting points were spatially random. For each starting point, a fiber streamline was grown in two opposite directions with a fixed step of 1 mm. Once the fiber entered a new voxel, the fiber growth continued along the ODF maximum direction that produces the least curvature for the fiber (i.e., was most similar to the trajectory of the fiber to that point). Fibers were stopped if the change in direction was greater than 60 degrees/mm. The process was complete when both ends of the fiber left the white matter mask.

Structural connectivity between pairs of regions was measured in terms of fiber density, defined as the number of streamlines between the two regions, normalized by the average length of the streamlines and average surface area of the two regions (Hagmann et al., 2008). The goal of this normalization was to compensate for the bias toward longer fibers inherent in the tractography procedure, as well as differences in region size.

A group structural connectivity matrix was constructed from the individual participants' matrices using a consensus approach. To preserve the edge length distribution in the individual participants' matrices, we first collated all extant edges in the individual matrices and binned them according to length. The number of bins was determined heuristically, as the square root of the mean binary density across participants. The consensus edges were then selected separately for each bin. For instance, if the mean number of edges (across participants) in a particular bin i is equal to k_i , we selected the k_i most commonly occurring edges in that bin. To ensure that inter-hemispheric edges are not systematically under-represented, this procedure was carried out separately for inter- and intra-hemispheric edges. The binary density of the final group matrix was 2.43%.

Functional Connectivity

Functional data were pre-processed using routines designed to facilitate subsequent network exploration (Murphy et al., 2009; Power et al., 2012). fMRI volumes were corrected for physiological variables, including regression of white matter, cerebrospinal fluid, as well as motion (three translations and three rotations, estimated by rigid body co-registration). BOLD time series were then subjected to a lowpass filter (temporal Gaussian filter with full width half maximum equal to 1.92 s). The first four time points were excluded from subsequent analysis to allow the time series to stabilize. Motion "scrubbing" was performed as described by Power et al. (2012).

A group-average functional connectivity matrix was constructed from the fMRI BOLD time series by concatenating the regional time series from all participants and estimating a single correlation matrix. To threshold this matrix, we sampled at random 276 points from the concatenated times series and calculated a full correlation matrix from these points. We repeated this analysis 1,000 times. From these bootstrapped samples, we estimated confidence intervals for the correlation magnitude between every pair of brain regions. Pairs whose correlation was consistently positive or negative across the 1,000 samples were retained (along with the sign and weight of the correlation) as putative functional connections.

Graph Theoretic Measures

All graph theoretic metrics and analyses were performed using the Brain Connectivity Toolbox (<http://sites.google.com/site/bctnet/>), including degree, closeness, path length, and edge-betweenness (Rubinov and Sporns, 2010).

Community Detection

Functional network communities (RSNs) were identified using a variant of the modularity maximization approach (Newman and Girvan, 2004; Rubinov and Sporns, 2011). This approach aims to uncover the community assignments of each node that maximize the quality function

$$Q(\gamma) = \frac{1}{m^+} \sum_{ij} [w_{ij}^+ - \gamma \cdot p_{ij}^+] \delta(\sigma_i, \sigma_j) - \frac{1}{m^+ + m^-} \sum_{ij} [w_{ij}^+ - \gamma \cdot p_{ij}^-] \delta(\sigma_i, \sigma_j) \quad (\text{Equation 2})$$

Here, w_{ij}^+ is the connectivity matrix containing only the positive correlations. Similarly, w_{ij}^- contains only correlation values less than zero. The term $p_{ij}^\pm = (s_i^\pm s_j^\pm) / (2m^\pm)$ represents the expected density of connections between nodes i and j given some null model (in this case, the configuration model), where $s_i^\pm = \sum_j w_{ij}^\pm$ and $m^\pm = \sum_{i,j} w_{ij}^\pm$. The variable σ_i is the community assignment of node i , and $\delta(\sigma_i, \sigma_j)$ is the Kronecker function and is equal to 1 when $\sigma_i = \sigma_j$ and is 0 otherwise. Finally, the parameter γ is the structural resolution parameter, and scales the relative importance of the null model, which allows us to uncover larger ($\gamma < 1$) or smaller ($\gamma > 1$) communities.

We scanned resolution parameters $\gamma = 0.5$ to $\gamma = 10$ in increments of 0.1 and, at each scale, ran the Louvain algorithm 250 times (Blondel et al., 2008) to identify partitions that produced large Q values. We focused on the communities generated at $\gamma = 1.5$. This scale was selected because the similarity (measured as the Z score of the rand index) averaged over all pairs of partitions generated at that scale exceeded that of all the other scales (Traud et al., 2011). Rather than treat any of the 250 partitions as representative, we chose to study the consensus partition, which we arrived at following the method presented in Bassett et al. (2013).

The resulting consensus partition, which is used in the main text, had a modularity score $Q(\gamma) = 0.61$ and contained $N_c = 8$ communities which we visually compared and matched to the topographical profiles of known RSNs, including the ventral attention (VA), fronto-parietal (FPN), salience (SAL), default mode (DMN), dorsal attention (DA), somato-motor (SM), visual (VIS), and temporal (TEM) networks (Figure S1B).

Structural network communities were identified in an analogous manner, such that the communities generated at resolution $\gamma = 1$ had a modularity score $Q(\gamma) = 0.64$ and contained $N_c = 12$ communities (Figure S1A).

Rich Club Detection

A rich club is a subgraph of high-degree nodes that are densely interconnected among each other above and beyond what would be expected on the basis of their degrees (Colizza et al., 2006). Rich club detection is performed across a range of degrees. For degree k , all nodes with degree $\leq k$ are removed from the network. The rich club coefficient $\phi(k)$ is the ratio of remaining connections to all possible connections (i.e., the density of the remaining subgraph). This ratio is simultaneously computed for a null distribution of 1,000 randomized networks with preserved degree sequences. The resulting null distribution of rich club coefficients is used to normalize the empirical rich club coefficient $\phi_{norm}(k) = \phi(k) / \phi_{random}(k)$. This procedure is repeated for a range of k . A $\phi_{norm}(k)$ that is consistently greater than 1 over a range of k suggests the existence of rich club organization. In the present study we observed consistent, statistically significant $\phi_{norm}(k) > 1$ for $k \geq 57$, resulting in a rich club with 15 nodes.

Having classified nodes as belonging to the rich club or not, we can classify edges in a similar way. Edges that connect non-rich club nodes to non-rich club nodes are classified as “local,” edges connecting non-rich club nodes to rich club nodes are classified as “feeder,” and edges connecting rich club nodes to other rich club nodes are classified as “rich club.”

Rewired Structural Networks

As an alternative null model to the label-permuting procedure reported in the Results section, we also created a population of randomized null networks, with preserved degree and strength sequences. The networks were first randomized by swapping pairs of edges, thus preserving binary degree (Maslov and Sneppen, 2002). In order to approximate the strength sequence of the observed structural connectivity matrix, we used a simulated annealing procedure in which we minimized a cost function defined as $E = \sum_i |s_i - s'_i|$, where s_i and s'_i are the strength of node i in the observed and randomized networks, respectively. To minimize this energy, we randomly permuted weight assign-

ments across edges and probabilistically accepted the permutations that reduced the energy while simultaneously reducing the temperature. The annealing schedule consisted of 10^7 iterations and a starting temperature of $t_0 = 100$, which was scaled by 0.125 after each iteration. The result of this procedure was an average final energy of $E = 3.27 \pm 0.53$, which indicates that the average strength discrepancy per node was slightly greater than 0.003.

We created Z scores for adoption times, cooperative speed-ups, competitiveness, and diversity based on this rewiring null model, and correlated them with Z scores derived from the permutation-based null model, as reported in the Results section. We find a good overall correspondence between the two sets of Z scores ($r = 0.74, 0.68, 0.46, \text{ and } 0.64$; $p < 0.01$ for all measures).

LTM

The LTM refers to a family of models that describe how a particular node in a network adopts a certain state if some proportion of its neighbors have also adopted that state (Granovetter, 1978). The state of a node i at time t is described by the variable $s_i(t) = \{0, 1\}$, such that the node has either adopted the active state (1) or not (0). Once a node adopts the active state, it remains active forever.

At time $t = 0$ the entire network is in an inactive state, save for a subset of nodes (“seeds”) that are activated, initializing a perturbation. In the synchronous update model, the state of every node i depends on its neighborhood N_i and is updated at every time step according to the following rule,

$$s_i(t+1) = \begin{cases} 1 & \text{if } \theta k_i < \sum_{j \in N_i} s_j(t) \\ 0 & \text{otherwise.} \end{cases} \quad (\text{Equation 3})$$

where θ denotes the threshold and k_i the degree of node i . As explained in the Results section, in the present study we set $\theta = 0.008$.

For binary networks, the threshold simply refers to the proportion of a node’s neighbors that must adopt the active state before the node adopts. For weighted networks, the threshold refers to the proportion of a node’s total weighted inputs that connect to nodes with active states before the node adopts the active state as well. In the present study, all but one of the results were generated using the synchronous update model on a weighted anatomical brain network, where the weights represent the fiber densities derived from computational tractography.

To infer the order in which individual edges are used during a cascade (Figures 1D and 1E), we used asynchronous updating. Here, the threshold rule operates on a weighted network as described above, but the influence of one neighbor on another is subject to a finite “transit time,” which we define as the ratio of fiber length to fiber density. This reflects the intuition that perturbations should spread faster along short, thick fiber tracts than on long, thin fiber tracts. The transit time makes it possible to unambiguously infer which particular connections contribute to change in state for any given node.

In the case of cooperative and competitive spreading we also make use of synchronous updating, using fiber densities to weigh the contribution of neighbors. In the competitive case, we simply extend the model to include two possible active states or “colors.” Once a node adopts a particular color, it remains in that specific active state forever. For a node to adopt a particular color, its weighted neighborhood must exceed the proportional threshold for that specific color; in other words, the colors cannot be combined to exceed a threshold. The weights provided by fiber densities help to break ties. Thus, in cases where both competing signals exceed threshold for a particular node, the node will adopt the signal that accounts for the greater total weight of its connections.

From these scenarios we define several performance metrics that characterize the spread of cascades. In the cooperative case, we define the speed-up (S) in adoption time in the two-seed case (A_{ij}) relative to the faster of the individual single-seed cases (A_i, A_j)

$$S = \frac{\min(A_i, A_j) - A_{ij}}{\min(A_i, A_j)}. \quad (\text{Equation 4})$$

For global speed-ups, A represents the mean adoption time for the whole network, while for local speed-ups, A represents the adoption time for a particular target node.

In the competitive case, we define the competitiveness of a node i as follows. If two competing cascades are initiated at nodes i and j , we define the competitiveness of node i as the size of the cascade initiated at node i , averaged over all nodes j . We define the diversity of a node in terms of the information entropy of its neighborhood. For a node i and a set of c possible node colors, we calculate the probability that the neighbors of i will adopt each state x_c and define the entropy h_i as

$$h_i = - \sum_c P(x_c) \log P(x_c). \quad (\text{Equation 5})$$

In the present case, where we consider only two possible active states (e.g., "red" and "blue"), the entropy of a node's neighborhood would be calculated as

$$h_i = - (P(\text{red}) \log P(\text{red}) + P(\text{blue}) \log P(\text{blue})) \quad (\text{Equation 6})$$

Finally, we define the conformity of a particular node as the probability of that node adopting a particular state given the final states of its neighbors. Thus, if a particular node has 5 neighbors, with 2/5 neighbors "red" and 3/5 neighbors "blue," and the node itself is "red," the conformity of that node is said to be 2/5.

SUPPLEMENTAL INFORMATION

Supplemental Information includes four figures and can be found with this article online at <http://dx.doi.org/10.1016/j.neuron.2015.05.035>.

AUTHOR CONTRIBUTIONS

B.M., R.F.B., and O.S. designed the research and wrote the paper. B.M. and R.F.B. performed the experiments. A.N., J.G., A.G., P.H., A.F., and Y.-Y.A. contributed data and analytic tools.

ACKNOWLEDGMENTS

O.S. was supported by the J.S. McDonnell Foundation (#220020387) and the National Science Foundation (#1212778). R.F.B. was supported by the National Science Foundation/Integrative Graduate Education and Research Traineeship Training Program in the Dynamics of Brain-Body-Environment Systems at Indiana University. B.M. was supported by a Natural Sciences and Engineering Research Council of Canada Postdoctoral Fellowship. J.G. was supported by the Indiana University Network Science Institute and the Indiana Alzheimer Disease Center (NIH/NIA P30 AG10133). Y.-Y.A. was supported by a Microsoft Research Faculty Fellowship. P.H. was supported by the Leenaards Foundation. A.G. was supported by the Swiss National Science Foundation (#320030_130090).

Received: March 3, 2015

Revised: April 15, 2015

Accepted: May 11, 2015

Published: June 17, 2015

REFERENCES

- Abdelnour, F., Voss, H.U., and Raj, A. (2014). Network diffusion accurately models the relationship between structural and functional brain connectivity networks. *Neuroimage* **90**, 335–347.
- Bassett, D.S., Greenfield, D.L., Meyer-Lindenberg, A., Weinberger, D.R., Moore, S.W., and Bullmore, E.T. (2010). Efficient physical embedding of topologically complex information processing networks in brains and computer circuits. *PLoS Comput. Biol.* **6**, e1000748.
- Bassett, D.S., Porter, M.A., Wymbs, N.F., Grafton, S.T., Carlson, J.M., and Mucha, P.J. (2013). Robust detection of dynamic community structure in networks. *Chaos* **23**, 013142.
- Beggs, J.M., and Plenz, D. (2003). Neuronal avalanches in neocortical circuits. *J. Neurosci.* **23**, 11167–11177.
- Betz, R.F., Griffa, A., Avena-Koenigsberger, A., Goñi, J., Thiran, J.-P., Hagmann, P., and Sporns, O. (2013). Multi-scale community organization of the human structural connectome and its relationship with resting-state functional connectivity. *Netw. Sci.* **1**, 353–373.
- Blondel, V.D., Guillaume, J.-L., Lambiotte, R., and Lefebvre, E. (2008). Fast unfolding of communities in large networks. *J. Stat. Mech.* <http://dx.doi.org/10.1088/1742-5468/2008/10/P10008>.
- Bullmore, E., and Sporns, O. (2012). The economy of brain network organization. *Nat. Rev. Neurosci.* **13**, 336–349.
- Cammoun, L., Gigandet, X., Meskaldji, D., Thiran, J.P., Sporns, O., Do, K.Q., Maeder, P., Meuli, R., and Hagmann, P. (2012). Mapping the human connectome at multiple scales with diffusion spectrum MRI. *J. Neurosci. Methods* **203**, 386–397.
- Centola, D. (2010). The spread of behavior in an online social network experiment. *Science* **329**, 1194–1197.
- Cole, M.W., Reynolds, J.R., Power, J.D., Repovs, G., Anticevic, A., and Braver, T.S. (2013). Multi-task connectivity reveals flexible hubs for adaptive task control. *Nat. Neurosci.* **16**, 1348–1355.
- Colizza, V., Flammini, A., Serrano, M.A., and Vespignani, A. (2006). Detecting rich-club ordering in complex networks. *Nat. Phys.* **2**, 110–115.
- Couzin, I.D., Krause, J., Franks, N.R., and Levin, S.A. (2005). Effective leadership and decision-making in animal groups on the move. *Nature* **433**, 513–516.
- Crossley, N.A., Mechelli, A., Vértes, P.E., Winton-Brown, T.T., Patel, A.X., Ginestet, C.E., McGuire, P., and Bullmore, E.T. (2013). Cognitive relevance of the community structure of the human brain functional coactivation network. *Proc. Natl. Acad. Sci. USA* **110**, 11583–11588.
- Daducci, A., Gerhard, S., Griffa, A., Lemkaddem, A., Cammoun, L., Gigandet, X., Meuli, R., Hagmann, P., and Thiran, J.P. (2012). The connectome mapper: an open-source processing pipeline to map connectomes with MRI. *PLoS ONE* **7**, e48121.
- Damoiseaux, J.S., Rombouts, S.A.R.B., Barkhof, F., Scheltens, P., Stam, C.J., Smith, S.M., and Beckmann, C.F. (2006). Consistent resting-state networks across healthy subjects. *Proc. Natl. Acad. Sci. USA* **103**, 13848–13853.
- Deco, G., Jirsa, V.K., Robinson, P.A., Breakspear, M., and Friston, K. (2008). The dynamic brain: from spiking neurons to neural masses and cortical fields. *PLoS Comput. Biol.* **4**, e1000092.
- Deco, G., Jirsa, V.K., and McIntosh, A.R. (2011). Emerging concepts for the dynamical organization of resting-state activity in the brain. *Nat. Rev. Neurosci.* **12**, 43–56.
- Delvenne, J.-C., Yaliraki, S.N., and Barahona, M. (2010). Stability of graph communities across time scales. *Proc. Natl. Acad. Sci. USA* **107**, 12755–12760.
- Desimone, R., and Duncan, J. (1995). Neural mechanisms of selective visual attention. *Annu. Rev. Neurosci.* **18**, 193–222.
- Estrada, E., and Hatano, N. (2008). Communicability in complex networks. *Phys. Rev. E Stat. Nonlin. Soft Matter Phys.* **77**, 036111.
- Fornito, A., Harrison, B.J., Zalesky, A., and Simons, J.S. (2012). Competitive and cooperative dynamics of large-scale brain functional networks supporting recollection. *Proc. Natl. Acad. Sci. USA* **109**, 12788–12793.
- Fries, P., Reynolds, J.H., Rorie, A.E., and Desimone, R. (2001). Modulation of oscillatory neuronal synchronization by selective visual attention. *Science* **291**, 1560–1563.
- Goñi, J., van den Heuvel, M.P., Avena-Koenigsberger, A., Velez de Mendizabal, N., Betzel, R.F., Griffa, A., Hagmann, P., Corominas-Murtra, B., Thiran, J.-P., and Sporns, O. (2014). Resting-brain functional connectivity predicted by analytic measures of network communication. *Proc. Natl. Acad. Sci. USA* **111**, 833–838.
- Granovetter, M. (1978). Threshold models of collective behavior. *Am. J. Sociol.* **83**, 1420–1443.
- Hagmann, P., Cammoun, L., Gigandet, X., Meuli, R., Honey, C.J., Wedeen, V.J., and Sporns, O. (2008). Mapping the structural core of human cerebral cortex. *PLoS Biol.* **6**, e159.
- Helbing, D., Farkas, I., and Vicsek, T. (2000). Simulating dynamical features of escape panic. *Nature* **407**, 487–490.

- Hellyer, P.J., Shanahan, M., Scott, G., Wise, R.J.S., Sharp, D.J., and Leech, R. (2014). The control of global brain dynamics: opposing actions of frontoparietal control and default mode networks on attention. *J. Neurosci.* *34*, 451–461.
- Henry, A.D., Pralat, P., and Zhang, C.Q. (2011). Emergence of segregation in evolving social networks. *Proc. Natl. Acad. Sci. USA* *108*, 8605–8610.
- Honey, C.J., Sporns, O., Cammoun, L., Gigandet, X., Thiran, J.-P., Meuli, R., and Hagmann, P. (2009). Predicting human resting-state functional connectivity from structural connectivity. *Proc. Natl. Acad. Sci. USA* *106*, 2035–2040.
- Insel, T.R., Landis, S.C., and Collins, F.S. (2013). Research priorities. The NIH BRAIN Initiative. *Science* *340*, 687–688.
- Jones, D.K., Knösche, T.R., and Turner, R. (2013). White matter integrity, fiber count, and other fallacies: the do's and don'ts of diffusion MRI. *Neuroimage* *73*, 239–254.
- Koch, C., and Ullman, S. (1987). Shifts in selective visual attention: towards the underlying neural circuitry. In *Matters of Intelligence in Synthese Library*, L. Vaina, ed. (Springer Netherlands), pp. 115–141.
- Kragel, J.E., and Polyn, S.M. (2015). Functional interactions between large-scale networks during memory search. *Cereb. Cortex* *25*, 667–679.
- Maslov, S., and Sneppen, K. (2002). Specificity and stability in topology of protein networks. *Science* *296*, 910–913.
- Menon, V., and Uddin, L.Q. (2010). Saliency, switching, attention and control: a network model of insula function. *Brain Struct. Funct.* *214*, 655–667.
- Messé, A., Hütt, M.-T., König, P., and Hilgetag, C.C. (2015). A closer look at the apparent correlation of structural and functional connectivity in excitable neural networks. *Sci. Rep.* *5*, 7870.
- Mišić, B., Goñi, J., Betzel, R.F., Sporns, O., and McIntosh, A.R. (2014a). A network convergence zone in the hippocampus. *PLoS Comput. Biol.* *10*, e1003982.
- Mišić, B., Sporns, O., and McIntosh, A.R. (2014b). Communication efficiency and congestion of signal traffic in large-scale brain networks. *PLoS Comput. Biol.* *10*, e1003427.
- Murphy, K., Birn, R.M., Handwerker, D.A., Jones, T.B., and Bandettini, P.A. (2009). The impact of global signal regression on resting state correlations: are anti-correlated networks introduced? *Neuroimage* *44*, 893–905.
- Nematzadeh, A., Ferrara, E., Flammini, A., and Ahn, Y.-Y. (2014). Optimal network modularity for information diffusion. *Phys. Rev. Lett.* *113*, 088701.
- Newman, M.E.J., and Girvan, M. (2004). Finding and evaluating community structure in networks. *Phys. Rev. E Stat. Nonlin. Soft Matter Phys.* *69*, 026113.
- O'Dea, R., Crofts, J.J., and Kaiser, M. (2013). Spreading dynamics on spatially constrained complex brain networks. *J. R. Soc. Interface* *10*, 20130016.
- Oh, S.W., Harris, J.A., Ng, L., Winslow, B., Cain, N., Mihalas, S., Wang, Q., Lau, C., Kuan, L., Henry, A.M., et al. (2014). A mesoscale connectome of the mouse brain. *Nature* *508*, 207–214.
- Pastor-Satorras, R., and Vespignani, A. (2001). Epidemic spreading in scale-free networks. *Phys. Rev. Lett.* *86*, 3200–3203.
- Power, J.D., Cohen, A.L., Nelson, S.M., Wig, G.S., Barnes, K.A., Church, J.A., Vogel, A.C., Laumann, T.O., Miezin, F.M., Schlaggar, B.L., and Petersen, S.E. (2011). Functional network organization of the human brain. *Neuron* *72*, 665–678.
- Power, J.D., Barnes, K.A., Snyder, A.Z., Schlaggar, B.L., and Petersen, S.E. (2012). Spurious but systematic correlations in functional connectivity MRI networks arise from subject motion. *Neuroimage* *59*, 2142–2154.
- Raj, A., Kuceyeski, A., and Weiner, M. (2012). A network diffusion model of disease progression in dementia. *Neuron* *73*, 1204–1215.
- Ritter, P., Schirner, M., McIntosh, A.R., and Jirsa, V.K. (2013). The virtual brain integrates computational modeling and multimodal neuroimaging. *Brain Connect.* *3*, 121–145.
- Roberts, J.A., Boonstra, T.W., and Breakspear, M. (2015). The heavy tail of the human brain. *Curr. Opin. Neurobiol.* *31*, 164–172.
- Rubinov, M., and Sporns, O. (2010). Complex network measures of brain connectivity: uses and interpretations. *Neuroimage* *52*, 1059–1069.
- Rubinov, M., and Sporns, O. (2011). Weight-conserving characterization of complex functional brain networks. *Neuroimage* *56*, 2068–2079.
- Rubinov, M., and Bullmore, E. (2013). Fledgling pathoconnectomics of psychiatric disorders. *Trends Cogn. Sci.* *17*, 641–647.
- Schelling, T.C. (1971). Dynamic models of segregation. *J. Math. Sociol.* *1*, 143–186.
- Seeley, W.W., Menon, V., Schatzberg, A.F., Keller, J., Glover, G.H., Kenna, H., Reiss, A.L., and Greicius, M.D. (2007). Dissociable intrinsic connectivity networks for salience processing and executive control. *J. Neurosci.* *27*, 2349–2356.
- Shen, K., Hutchison, R.M., Bezgin, G., Everling, S., and McIntosh, A.R. (2015). Network structure shapes spontaneous functional connectivity dynamics. *J. Neurosci.* *35*, 5579–5588.
- Smith, S.M., Fox, P.T., Miller, K.L., Glahn, D.C., Fox, P.M., Mackay, C.E., Filippini, N., Watkins, K.E., Toro, R., Laird, A.R., and Beckmann, C.F. (2009). Correspondence of the brain's functional architecture during activation and rest. *Proc. Natl. Acad. Sci. USA* *106*, 13040–13045.
- Stam, C.J. (2014). Modern network science of neurological disorders. *Nat. Rev. Neurosci.* *15*, 683–695.
- Stam, C.J., van Straaten, E.C.W., Van Dellen, E., Tewarie, P., Gong, G., Hillebrand, A., Meier, J., and Van Mieghem, P. (2015). The relation between structural and functional connectivity patterns in complex brain networks. *Int. J. Psychophysiol.* Published online February 10, 2015. <http://dx.doi.org/10.1016/j.ijpsycho.2015.02.011>.
- Thomas, C., Ye, F.Q., Irfanoglu, M.O., Modi, P., Saleem, K.S., Leopold, D.A., and Pierpaoli, C. (2014). Anatomical accuracy of brain connections derived from diffusion MRI tractography is inherently limited. *Proc. Natl. Acad. Sci. USA* *111*, 16574–16579.
- Traud, A.L., Kelsic, E.D., Mucha, P.J., and Porter, M.A. (2011). Comparing community structure to characteristics in online collegiate social networks. *SIAM Rev.* *53*, 526–543.
- van den Heuvel, M.P., Kahn, R.S., Goñi, J., and Sporns, O. (2012). High-cost, high-capacity backbone for global brain communication. *Proc. Natl. Acad. Sci. USA* *109*, 11372–11377.
- Van Essen, D.C., Smith, S.M., Barch, D.M., Behrens, T.E.J., Yacoub, E., and Ugurbil, K.; WU-Minn HCP Consortium (2013). The WU-Minn human connectome project: an overview. *Neuroimage* *80*, 62–79.
- Vicsek, T., Czirók, A., Ben-Jacob, E., Cohen, I., and Shochet, O. (1995). Novel type of phase transition in a system of self-driven particles. *Phys. Rev. Lett.* *75*, 1226–1229.
- Watts, D.J. (2002). A simple model of global cascades on random networks. *Proc. Natl. Acad. Sci. USA* *99*, 5766–5771.
- Wedeer, V.J., Hagmann, P., Tseng, W.Y., Reese, T.G., and Weisskoff, R.M. (2005). Mapping complex tissue architecture with diffusion spectrum magnetic resonance imaging. *Magn. Reson. Med.* *54*, 1377–1386.
- Wedeer, V.J., Wang, R.P., Schmahmann, J.D., Benner, T., Tseng, W.Y.I., Dai, G., Pandya, D.N., Hagmann, P., D'Arceuil, H., and de Crespigny, A.J. (2008). Diffusion spectrum magnetic resonance imaging (DSI) tractography of crossing fibers. *Neuroimage* *41*, 1267–1277.
- Wolpert, D.M., and Ghahramani, Z. (2000). Computational principles of movement neuroscience. *Nat. Neurosci.* *3* (Suppl.), 1212–1217.
- Womelsdorf, T., Schoffelen, J.-M., Oostenveld, R., Singer, W., Desimone, R., Engel, A.K., and Fries, P. (2007). Modulation of neuronal interactions through neuronal synchronization. *Science* *316*, 1609–1612.
- Yeo, B.T., Krienen, F.M., Sepulcre, J., Sabuncu, M.R., Lashkari, D., Hollinshead, M., Roffman, J.L., Smoller, J.W., Zöllei, L., Polimeni, J.R., et al. (2011). The organization of the human cerebral cortex estimated by intrinsic functional connectivity. *J. Neurophysiol.* *106*, 1125–1165.
- Zalesky, A., Fornito, A., Cocchi, L., Gollo, L.L., and Breakspear, M. (2014). Time-resolved resting-state brain networks. *Proc. Natl. Acad. Sci. USA* *111*, 10341–10346.
- Zhou, C., Zemanová, L., Zamora, G., Hilgetag, C.C., and Kurths, J. (2006). Hierarchical organization unveiled by functional connectivity in complex brain networks. *Phys. Rev. Lett.* *97*, 238103.